

Structural and functional integrity of decontaminated N95 respirators: Experimental results

2022, Vol. 51(5S) 7999S–8017S



© The Author(s) 2022

Article reuse guidelines:

sagepub.com/journals-permissions

DOI: 10.1177/15280837221082322

journals.sagepub.com/home/jit

Sumit Sharma¹, Fang Wang², Shubham Kumar¹,
Ruchika R Nawal³, Priya Kumar⁴, Sudha Yadav³, Imre Szent⁵,
Akos Kukovecz⁵, Ulf D Schiller²  and Amit Rawal¹ 

Abstract

With the recent emergence of highly transmissible variants of the novel coronavirus SARS-CoV-2, the demand for N95 respirators is expected to remain high. The extensive use of N95 respirators by the public is susceptible to demand-supply gaps and raises concern about their disposal, threatening the environment with a new kind of plastic pollution. Herein, we investigated the filtration performance of the N95 respirator by specifically analyzing the structure in the key filtration layers of meltblown nonwoven after decontamination with one and five cycles of liquid hydrogen peroxide, ultraviolet radiation, moist heat, and aqueous soap solution treatments. With the aid of X-ray microcomputed tomography (microCT) analysis, the *local* structural heterogeneity of the meltblown nonwoven has been unfolded and subsequently correlated with their filtration performance at a face velocity that matched with speaking conditions (~3.89 m/s). The filtration efficiency results of the N95 respirator remain unaltered after performing one cycle of treatment modalities (except autoclave).

¹Department of Textile and Fibre Engineering, Indian Institute of Technology Delhi, Delhi, India

²Department of Materials Science and Engineering, Clemson University, Clemson, SC, USA

³Department of Conservative Dentistry & Endodontics, Maulana Azad Institute of Dental Sciences, New Delhi, India

⁴Department of Oral Pathology, Maulana Azad Institute of Dental Sciences, New Delhi, India

⁵Interdisciplinary Excellence Centre, Department of Applied and Environmental Chemistry, University of Szeged, Szeged, Hungary

Corresponding author:

Amit Rawal, Department of Textile and Fibre Engineering, Indian Institute of Technology Delhi, Hauz Khas, New Delhi 110016, India.

Email: arawal@iitd.ac.in

Keywords

N95 respirator, decontamination treatments, meltblown nonwovens, X-ray microCT analysis

Introduction

With the recent emergence of highly transmissible SARS-CoV-2 variants 501Y.V1 (B.1.1.7) in the United Kingdom [1], 501Y.V2 (B.1.351), B.1.1.529 in South Africa [2,3], and B.1.617 in India [4], the World Health Organization (WHO) has strongly recommended the use of face masks for the general public [5,6]. Specifically, the use of N95 respirators has become an essential component to protect the front-line workers from contracting the deadly virus. Therefore, the demand for N95 respirators is expected to remain high, increasing the susceptibility to the demand-supply gaps and an environmental threat from a new kind of plastic pollution [7]. N95 respirators are multi-layered textile materials with key filtration layers of meltblown nonwoven material comprising fine polypropylene fibers that are cost-effective, chemically robust, and easily scalable to multiple fiber length scales [8]. Therefore, it is highly pertinent that the healthcare community continues to uncover innovative ways to overcome the short supply of N95 respirators [9]. Sterilization and decontamination of face masks have recently emerged as highly resourceful methods to fulfill the limited supply of masks and respirators [10,11]. Several decontamination methods and chemical treatments, including ultraviolet radiation, hydrogen peroxide vapor, liquid hydrogen peroxide, ethylene oxide, moist heat incubation, ethanol, microwave-generated steam, rice-cooker steam, and many others, have been reported as potential ways to treat N95 respirators for their re-usability [12–22]. Although all the decontamination methods have not been tested for filtration performance or against SARS-CoV-2, the expired N95 masks reprocessed using ethylene oxide sterilization maintained excellent filtration efficiency under laboratory conditions [10].

Recently, seven different methods, including autoclave treatment, ethylene oxide gas treatment, low-temperature hydrogen peroxide gas plasma treatment, vaporous hydrogen peroxide exposure, peracetic acid dry fogging, ultraviolet C irradiation, and moist heat treatment, were used to decontaminate a range of N95 masks after contamination with SARS-CoV-2 virus as a surrogate [23]. Surprisingly, most of these treatments have not only successfully deactivated the SARS-CoV-2 virus, but all N95 masks sustained one cycle of all treatment modalities without loss of functional or structural integrity. However, the structural integrity of decontaminated N95 respirators should be assessed by analyzing the internal structure of key filtration layers and/or via understanding the particle penetration and capture mechanisms. Recently, Vejerano and Ahn [24] suggested that the filtration performance of decontaminated N95 respirators should be carried out under velocities representative of normal to active breathing conditions. Significant proportions of infectious particles are generated and spread by speaking or coughing at velocities up to 100 times greater than set under the standard test conditions [25]. Various testing methods and publications do not clearly specify the face velocity but instead

provide a volumetric flow rate for generating particles [25]. Therefore, it is essential to evaluate the filtration performance of decontaminated N95 respirators at a face velocity that emulates speaking or coughing conditions and simultaneously analyze the structure of the key filtration layers.

Therefore, the central aim of this work was to investigate the morphology of the meltblown nonwoven layers present in an N95 respirator after decontaminating with one and five cycles of liquid hydrogen peroxide, ultraviolet radiation, moist heat, and aqueous soap solution and subsequently correlating with their filtration performance at a face velocity (~ 3.89 m/s) that emulates speaking conditions [26]. With the aid of X-ray microcomputed tomography (microCT) analysis, the variation in the morphological characteristics has been analyzed to monitor the local inhomogeneities, which has not been investigated in the literature. Specifically, X-ray microCT served to quantify various fiber and structural parameters of decontaminated meltblown nonwoven layers, namely, three-dimensional (3D) fiber orientation distribution, porosity, and pore size distribution. The multifold novel aspects of the present work can be realized by proposing strategies that mitigate the short supply of N95 respirators and assist in choosing the facile, scalable, and inexpensive decontamination treatment. Another merit of this work can be construed as an alternative solution to overcome the challenges of single-use plastics creating the most serious environmental threat [27].

Materials and methods

This in vitro study was carried out on a commercially available National Institute for Occupational Safety and Health (NIOSH)-approved Venus V-4400 disposable N95 flat-fold respirator. This N95 flat-fold respirator is composed of a single layer of needle-punched, two layers of spunbonded, and four layers of meltblown nonwoven materials (see Figure 1). The meltblown nonwoven layers comprising polypropylene fibers sandwiched between the inner and outer layers act as the ultra-fine microfilter, and thus, are key functional components of the N95 respirators. Further details of the meltblown nonwoven layers have been provided in Table 1. The control (untreated) and treated respirators were evaluated by carefully separating various layers of the respirators.

As aforementioned, the filtration performance of the N95 respirators was assessed after treating with one and five cycles of various decontamination methods, including treatment with an aqueous solution of hydrogen peroxide (H_2O_2), aqueous soap solution, autoclaving, and ultraviolet (UV) light. The details of decontamination methods are given below.

Decontamination by H_2O_2 : Here, the N95 respirator was decontaminated using an aqueous solution of H_2O_2 . Samples were dipped in 3 wt.% aqueous H_2O_2 (Y K Laboratories, India) for 30 min, followed by drying at room temperature.

Decontamination by soap solution: N95 respirators were immersed in warm soapy water solution of a concentration of 1 g/L (made using Dettol bar soap, Reckitt Benckiser, India) for 10 min at 40°C followed by 72 h of drying.

Decontamination by UV treatment: N95 respirators were irradiated with 15 W ultraviolet C (UV-C) light at 254 nm for 15 min per surface. Respirators were placed on the

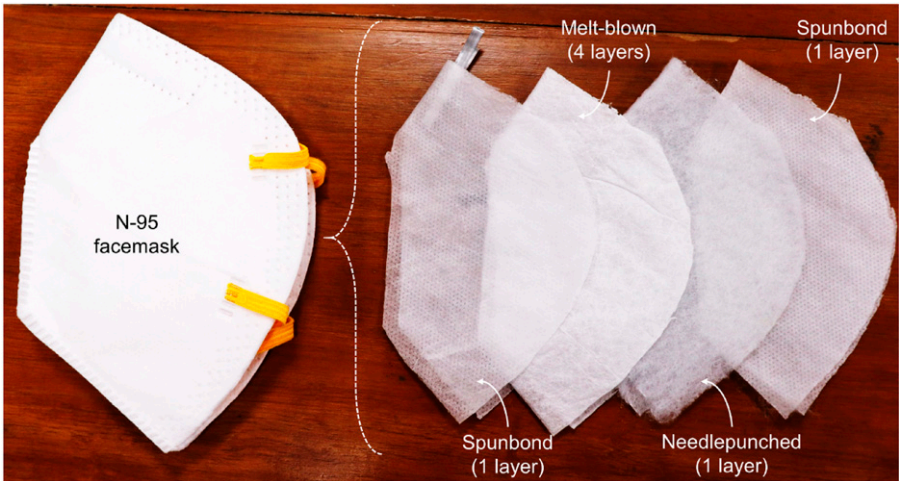


Figure 1. Constituent nonwoven layers of N95 respirator.

Table 1. Specifications of meltblown layers of the N95 respirator.

Particulars	Units	Meltblown layers
Fiber type	—	Polypropylene
Mass per unit area, m	g/m^2	45.91
Thickness, t	mm	0.58
Fiber density, ρ_f	kg/m^3	910
Porosity	—	0.91 (gravimetric, ε_g)
	—	0.88 (CTAn, ε_{CTAn})
Mean fiber diameter	μm	4.8 (SEM)

working surface of the UV-C sterilization chamber (S K Dent, India) fitted with a 15-W ultraviolet light for decontamination.

Decontamination by autoclaving: N95 respirators were sealed in an autoclave bag and treated in a steam pressure sterilizer (Sting II Class B autoclave) at 121°C for 15 min, followed by drying at room temperature.

The sample IDs were assigned based on the type of treatment (H_2O_2 denotes hydrogen peroxide, SO refers to soap, UV indicates ultraviolet light, and AU implies the autoclave) followed by the number of cycles. For instance, sample ID AU-5X denotes that the sample was treated with five cycles of autoclave treatment.

Filtration efficiency was measured at three distinct regions of each sample on the equipment shown schematically in Figure 2(a), using the particle size distribution shown in Figure 2(b). Here, the N95 respirator was mounted on a circular sample port of 1.65 cm diameter (area of 2.14 cm^2), which was connected to the particle counter (Model 9350-03, TSI Inc., USA). The ambient air was passed through the sample at a rate of 50 L/min for

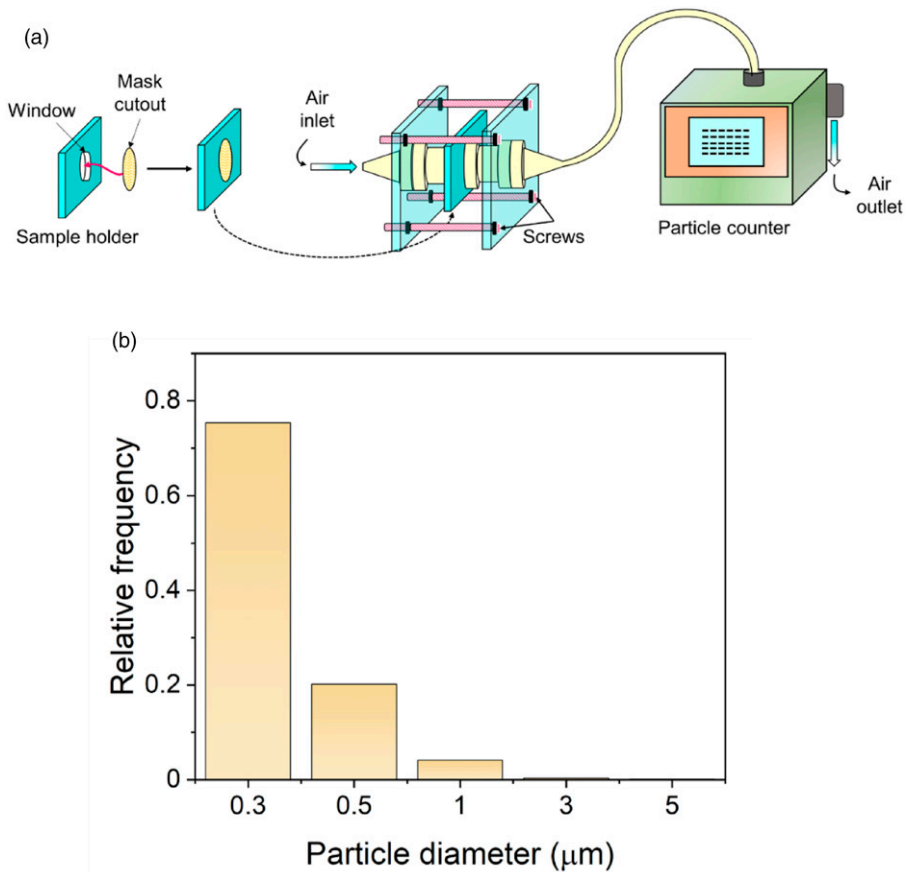


Figure 2. (a) Schematic of the apparatus used for the measurement of filtration efficiency and (b) particle size distribution used for filtration efficiency measurement.

5 min, and the particle counts for sizes of 0.3, 0.5, 1, 3, and 5 μm were recorded. To determine the filtration efficiency, the particle counts in the room were recorded before and after the filtration test under the same conditions. The filtration efficiency (η) of N95 flat-fold respirators was determined by measuring the change in particle concentration with and without filter medium using the equation [28]

$$\eta(\%) = \left(1 - \frac{N_o}{N_i}\right) * 100\% \quad (1)$$

where N_o and N_i are the total number of particles of a particular size measured with and without filter medium in the filter holder, respectively.

The difference in filtration efficiency due to changes in counts in the air remained within $\pm 0.5\%$. Further, the differential pressure was measured on a pressure drop analyzer

(Model NFA, New York Instruments, USA) separately so that there is no particle loss at the time of particle counting. Note that the face velocity of air used for filtration efficiency and differential pressure test was kept at 3.89 m/s, which matches well with the speaking conditions [26].

X-ray microcomputed tomography analysis

3D structural analysis of the swatches of meltblown nonwoven layers of N95 respirators before and after decontamination treatments was performed using the state-of-the-art Bruker Skyscan 2211 X-ray nano-computed tomography system. Here, the scans were performed while the sample stage was rotated for 180° in 0.12° steps to obtain 2300–2400 images with a resolution of $0.5 \mu\text{m}/\text{pixel}$. The X-rays were made to focus on the mounted specimen for 450 ms at each step using a tungsten target with a 40-kV source voltage and 800 μA current. Subsequently, various attributes of the scanned images were enhanced by employing defect pixel masking and ring artefact reduction techniques, which were performed in NRecon[®] (SkyScan, Bruker, Belgium). Further analysis was carried out by rotating the sample in one of the principal directions and binarizing the image dataset, using DATAVIEWER[®] (Bruker, Belgium) and CTAn[®] (Bruker, Belgium), respectively. The three-dimensional (3D) volumes were generated from the binarized dataset using CTVox[®] (Bruker, Belgium). A volume of interest (VOI) was chosen judiciously in order to avoid boundary irregularities [29,30].

The “structure thickness” employed under the “3D analysis” module on CTAn[®] provided the number-based distribution of the object diameter. In the binarized image dataset, the white-colored material was referred to as fibers, and the values of fiber diameters were obtained from the structure thickness values by applying “3D analysis” module on binarized VOI [29,30]. The pore diameters were obtained in a similar manner after converting the pore phase into the material phase and vice-versa. The number-based distributions were subsequently converted into frequency distributions to obtain the pore diameters and their corresponding distributions of the meltblown nonwoven layers [29,30]. The percentage object volume returned by the “3D analysis” module in CTAn[®] is the ratio of the number of voxels occupied by the fibers to the total number of voxels in the selected VOI [29,30]. This percentage object volume, therefore, corresponds to the fiber volume fraction (V_f) of the meltblown layers. Thus, the porosity (ε) was subsequently computed using the well-known relationship, i.e., $\varepsilon = 1 - V_f$. The porosity values of control and decontaminated meltblown layers have also been ascertained using the Digital Materials Laboratory Software (GeoDict[®]). Further details of Geodict based analysis can be obtained from ref. [31]. In general, the porosity values of control and decontaminated samples obtained via CTAn and Geodict analyses are in good agreement. The “individual 3D object analysis” module on CTAn[®] provided the in-plane and out-of-plane orientation angles of the individual objects (fibers in our case). These values of fiber orientation angles were translated into frequency distributions using Microsoft Excel and MATLAB R2020a to obtain the corresponding fiber orientation distributions.

Results and discussion

N95 respirators are multi-layered materials comprising meltblown, needlepunched, and spunbonded nonwovens, as shown in Figure 1. While the outer layer of spunbonded

nonwoven materials is designed to be hydrophobic in order to repel pathogen-containing droplets, the inner layer is made hydrophilic through surfactant treatment for enhanced wearer comfort. The thicker and stiffer needlepunched nonwoven layer can be molded into the desired shapes and is expected to perform as a pre-filter. The filtration performance is spearheaded by the multiple layers of meltblown nonwoven material comprising low-cost and chemically resistant polypropylene fibers [8]. The filtration efficiency and pressure drop values of the N95 respirator for particle size of 0.3 μm , determined before and after performing the decontamination treatments, are depicted in Figure 3.

Meltblown nonwovens are highly porous media composed of a three-dimensional (3D) network of fibers having diameters in the range of 1-10 μm [32]. The structural integrity of

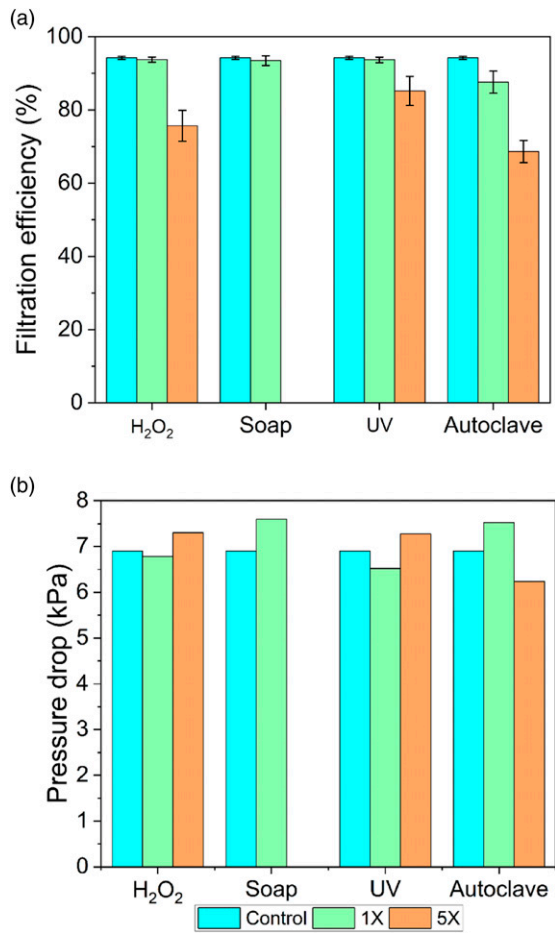


Figure 3. (a) Filtration efficiency of the N95 respirator for particle size of 0.3 μm . (b) Pressure drop across N95 respirator determined before and after performing the decontamination procedure. Note that the sample area used for the measurement of pressure drop was 2.14 cm^2 .

the meltblown nonwoven layers after decontamination is instrumental in maintaining the filtration performance of N95 respirators [15]. This demands a comprehensive evaluation of the local structural parameters of meltblown layers of N95 respirators before and after decontamination treatments. The three-dimensional (3D) structure of the meltblown layers of the N95 respirators before and after the first and fifth cycles of H_2O_2 , soap, UV, and autoclave treatments has been unfolded using the state-of-the-art X-ray microCT analysis, as depicted in Figure 4. These volumes were generated using the data obtained from the X-ray microCT scans. In particular, Figure 4 illustrates a visual comparison between the control (untreated) and treated samples that endured one and five cycles of various decontamination methods. Our visual results revealed that the structural integrity

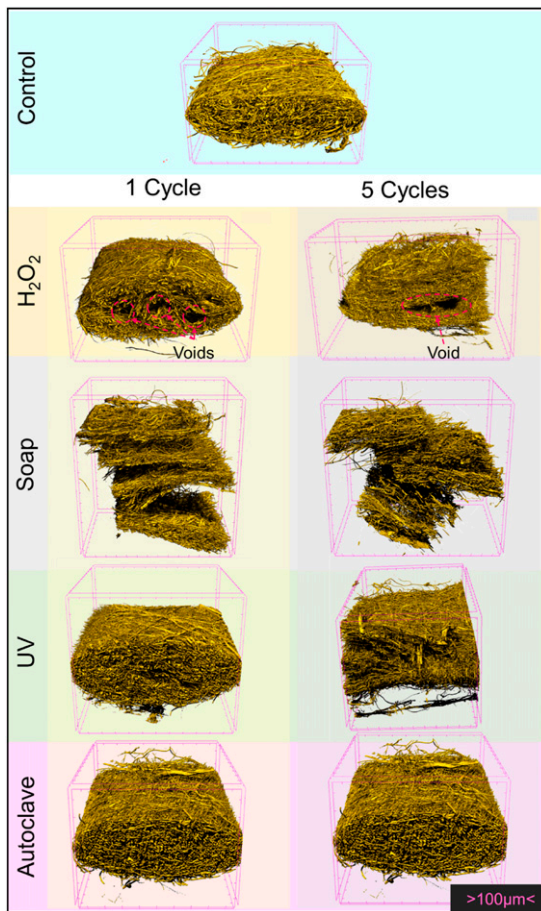


Figure 4. 3D-rendered volumes of meltblown nonwoven layers of N95 respirator before (control) and after one and five cycles of H_2O_2 , soap, UV, and autoclave treatments. Here, one division in the bounding box of figures indicates 100 μm .

appears to be preserved in autoclave-treated meltblown nonwovens followed by ultra-violet treatment. Liquid hydrogen peroxide delaminated the meltblown layers after five treatment cycles, whereas the loss of structural integrity was evident after the first cycle of aqueous soap treatment. However, our data also indicated modest variations in the magnitudes of filtration efficiency of the N95 respirator for particle sizes of 0.5, 1, 3 and 5 μm after treatment with various decontamination methods, as shown in Table 2. With the aid of scanning electron microscopy (SEM), a visual comparison between the control (untreated) and treated samples that endured one and five cycles of various decontamination methods has also been made, as illustrated in Figure 5. Intriguingly, the entrapment of soap particles can be seen after soap decontamination cycles.

Effect of H_2O_2 decontamination treatment

In the literature, contrary views have emerged on whether solution-based treatments can affect the structure and filtration performance of meltblown nonwoven materials [13,32]. One of the ways to determine the variations in the solution-treated meltblown was suggested on the basis of structural integrity and its relationship with the pressure drop [32]. Figure 4 illustrates the creation of voids in the meltblown layers after the first cycle of H_2O_2 treatment. Such voids yielded an increase in the overall porosity and enhanced local pore sizes, as shown in Figures 6(a) and (b). However, the rise in voids did not significantly deteriorate the overall filtration efficiency and pressure drop of the N95 respirator after the first cycle of H_2O_2 treatment (see Figure 3). Viscusi et al. [33] also reported insignificant differences in the filtration performance of N95 respirator after being treated with 3% liquid hydrogen peroxide solution. Further, the in-plane fiber orientation distribution after the first treatment cycle did not show any significant variation compared to the control sample (see Figure 6(c)). However, the spatial movement of fibers in the Z-direction led to a realignment of the fibers in the thru-thickness direction,

Table 2. Filtration efficiency (η) of N95 respirator for particles sizes of 0.5, 1, 3 and 5 μm observed before and after treating with various decontamination methods.

Sample ID	Particle size (μm)			
	0.5	1	3	5
Control	99.1	98.4	97.4	97.9
H_2O_2 -1X	99.3	98.7	97.8	98.4
H_2O_2 -5X	99.0	98.4	95.8	96.0
SO-1X	99.0	97.9	95.3	92.2
SO-5X	Blocked			
UV-1X	98.9	98.3	97.7	98.6
UV-5X	99.0	98.3	97.9	99.0
AU-1X	99.4	99.3	98.6	98.8
AU-5X	97.0	95.9	94.2	96.6

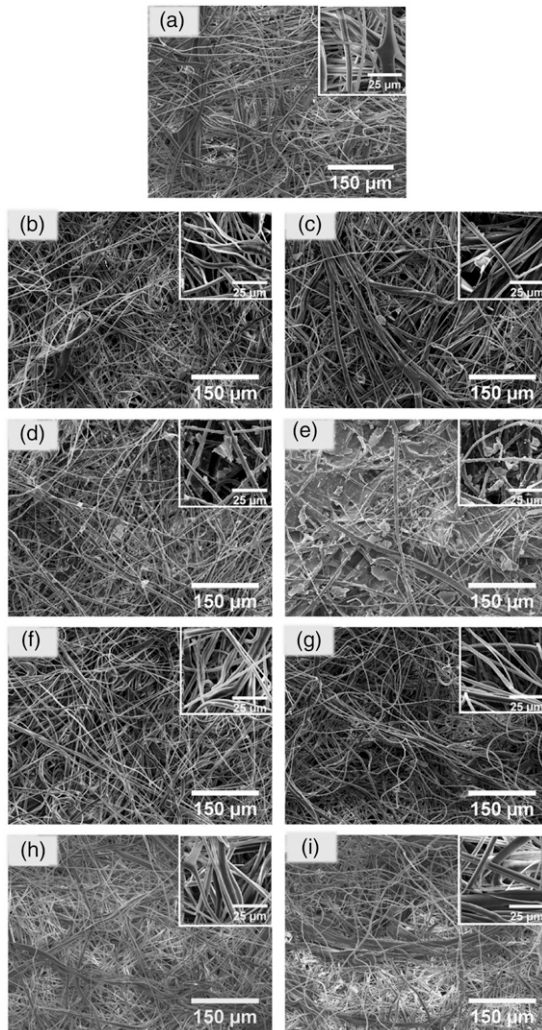


Figure 5. SEM micrographs of meltblown specimens of control and decontaminated samples. Here (a) refers to the control sample, whereas (b), (d), (f), and (h) refer to one cycle of decontamination treatment of H_2O_2 , soap, UV, and autoclave decontamination treatments, respectively. Similarly, (c), (e), (g), and (i) refer to five cycles of decontamination treatment of H_2O_2 , soap, UV, and autoclave decontamination treatments, respectively.

as evident from the out-of-plane fiber orientation distributions after treatment cycles (see [Figure 6\(d\)](#)).

After performing five cycles of H_2O_2 treatment, there was a significant reduction in porosity and local pore sizes. The experimental filtration efficiency showed a significant

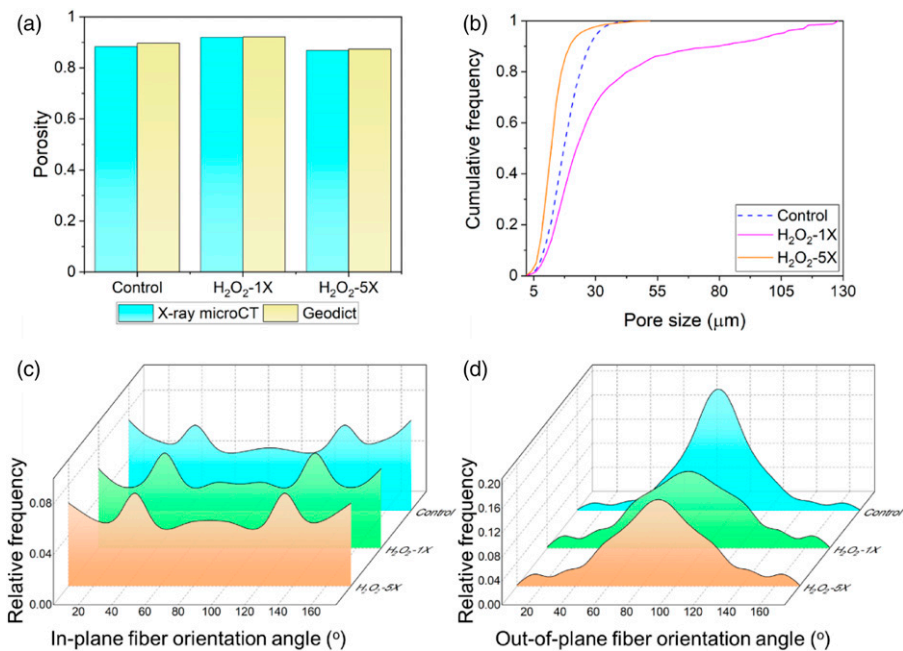


Figure 6. Elucidating the role of H₂O₂ treatment on (a) porosity, (b) pore size distribution, (c) in-plane fiber orientation distribution, and (d) out-of-plane fiber orientation distribution. Here, 90° angle in the out-of-plane fiber orientation distribution refers to the planar or in-plane direction and X-ray microCT implies the use of CTAn® software.

deterioration after five cycles of H₂O₂ treatment. This can be ascribed to delamination of certain layers of meltblown nonwoven material after five cycles of H₂O₂ treatment, as depicted in Figure 4. The loss of structural integrity also corroborates well with the rise in the magnitudes of pressure drop of the respirator (see Figure 3(b)). Further, the realignment of fibers in the thru-thickness direction can reduce the filtration efficiency, as demonstrated in simulations earlier [34]. These results demonstrated that the filtration performance of the N95 respirator after treating with five cycles of liquid hydrogen peroxide could be compromised by the loss of structural integrity of the meltblown layer.

Effect of soap decontamination treatment

Decontaminating the layers of N95 respirators with soap treatment was detrimental to their structural integrity. It can be seen that the structural damage after the repeated cycles of soap treatment amounted to the separation of layers (see Figure 4). Even a single cycle of soap treatment resulted in a higher pressure drop and the delamination of the meltblown layers, as evident from Figures 3(b) and 4. The separation of layers gave rise to larger voids leading to higher porosity and broader pore size distribution, as shown in Figures 7(a) and (b).

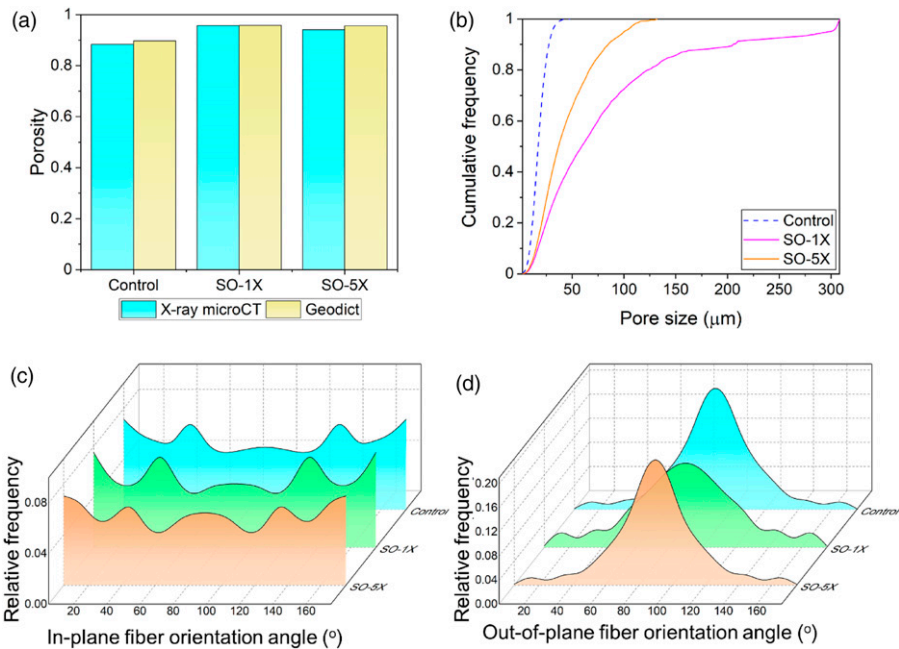


Figure 7. Elucidating the role of soap treatment on (a) porosity, (b) pore size distribution, (c) in-plane fiber orientation distribution, and (d) out-of-plane fiber orientation distribution. Here, 90° angle in the out-of-plane fiber orientation distribution refers to the planar or in-plane direction and X-ray microCT implies the use of CTAn® software.

Surprisingly, no significant variation in the fiber orientation of meltblown layers was observed even after five cycles of soap treatment (see [Figures 7\(c\) and \(d\)](#)). However, the filtration performance of the N95 respirators after five cycles of soap treatment could not be determined experimentally due to a very high pressure drop. To identify plausible reasons, we analyzed individual layers of the N95 respirators that revealed the entrapment of the soap particles in the meltblown layers after five cycles (see [Figure 5](#)). In general, our findings revealed that the filtration performance of the N95 respirator was significantly compromised after soap treatment, which also matched well with the results reported in the literature [20,35].

Effect of UV decontamination treatment

Exposure to UV radiation can be a promising way to decontaminate the N95 respirator, though it kills the SARS-CoV-2 slowly [23,36]. The number of disinfection cycles and UV dosage levels play a pivotal role in inactivating pathogens [13,37,38]. In this research work, ultraviolet light utilized the short electromagnetic waves (254 nm), a well-established concept to kill viruses [38]. Similar to the results reported by Liao et al. [32], the filtration efficiency remains unaffected after one cycle of UV treatment, as depicted in [Figure 3\(a\)](#). The filtration performance after treating with UV corroborated

well with the visual observation that revealed insignificant changes within the meltblown layers (see Figure 4). Although a narrow pore size distribution of single-cycle UV-treated meltblown layers was observed, there was no change in the overall porosity and in-plane fiber orientation distribution compared to the control sample, as depicted in Figures 8(a)–(c).

With the aid of X-ray microCT analysis, the meltblown layers have been unfolded after five cycles of UV treatment, as illustrated in Figure 4. It can be clearly observed that the layers of meltblown nonwoven disintegrated, which resulted in reducing the filtration efficiency and enhancing the pressure drop (see Figure 3). Such a disintegration of the layers resulted in the dilation of the structure leading to a slight increase in porosity while maintaining the local pore sizes within the layers. Although the fragmentation of layers tended to alter the out-of-plane direction of fibers, the spatial orientation of in-plane fibers remained the same (see Figures 8(c) and (d)). Historically, the UV radiation with distinct dosage levels has been effective in neutralizing the viruses but primarily on the surface of the masks [38–41]. Polypropylene fibers are UV absorbers, which transcends uncertainty about the deactivation of the smaller viral particles present in the inner layers of the respirator [32]. Moreover, higher magnitudes of UV dosage have been found to deteriorate the layers of the respirators [32,37,38].

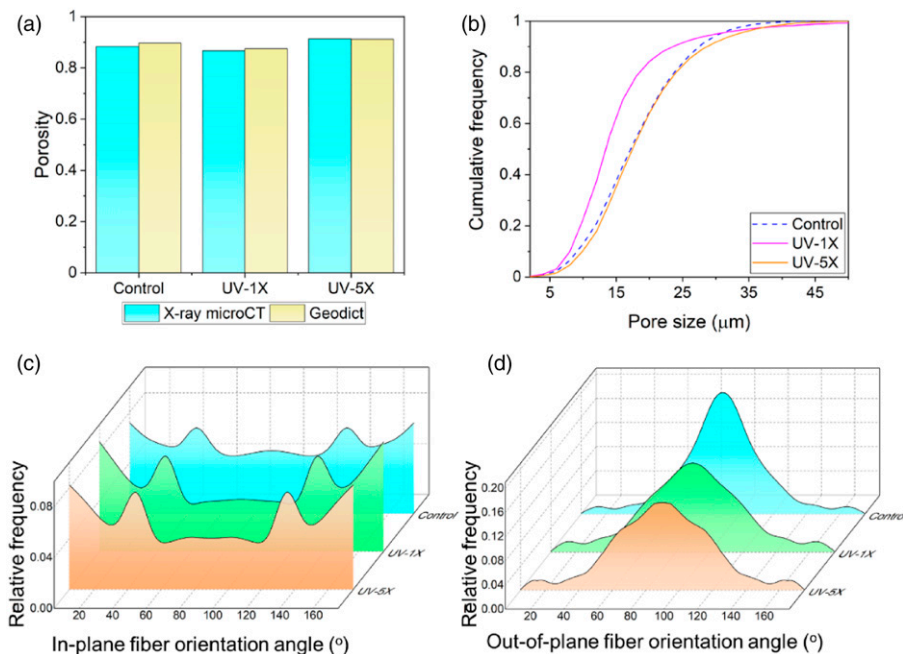


Figure 8. Elucidating the role of UV treatment on (a) porosity, (b) pore size distribution, (c) in-plane fiber orientation distribution, and (d) out-of-plane fiber orientation distribution. Here, 90° angle in the out-of-plane fiber orientation distribution refers to the planar or in-plane direction and X-ray microCT implies the use of CTAn® software.

Effect of autoclave decontamination treatment

Sterilization by steam is a well-established non-toxic, cost-effective, and scalable method successfully deployed in healthcare settings for microbial destruction [38,42]. Recently, some reports have demonstrated the complete inactivation of SARS-CoV-2 by moist heat treatment [23,43]. Several types of N95 respirators did not reveal any apparent degradation or loss of fit even at a temperature set at 121°C in the autoclave [44]. In this work, autoclaving has emerged as one of the least damaging decontaminating methods that resulted in the limited degradation of the meltblown layers of the N95 respirator. Through X-ray microCT analysis, the layers of meltblown nonwoven were stratified, and intriguingly, no notable damage was visible even after several cycles of treatment (see Figure 4). There was a decrease in the filtration efficiency of the respirator along with the reduction in the overall porosity and the pore size of meltblown layers after one cycle of autoclave treatment, as shown in Figures 3, 9(a) and 9(b). It should be noted that the morphological changes of meltblown layers can also be observed via the repositioning of fibers in the out-of-plane direction. Unexpectedly, the porosity and pore size distribution matched those of the control sample after five cycles of autoclave treatment, as shown in Figures 9(a) and (b). However, minimal changes were observed in the alignment of the

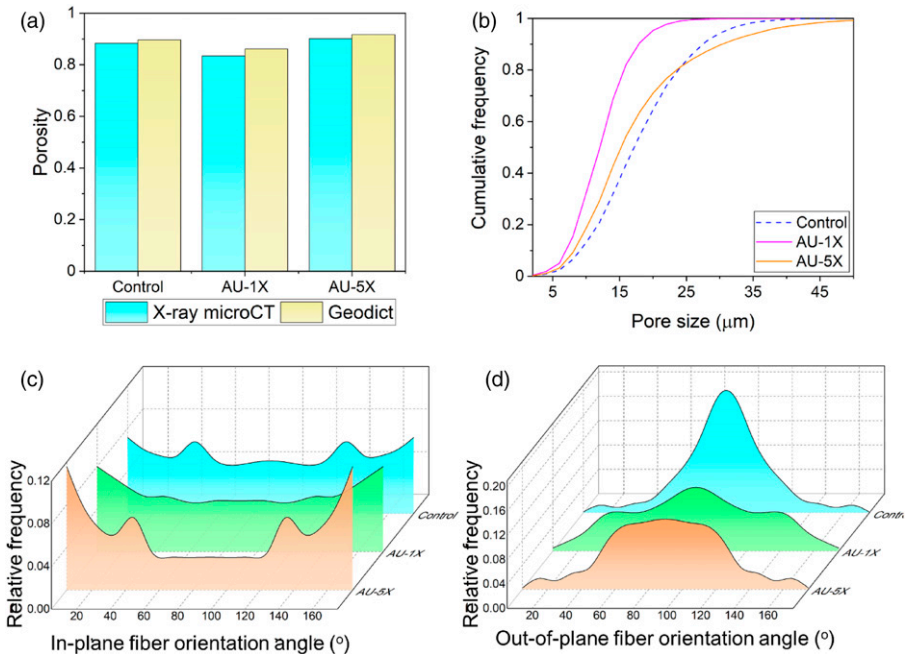


Figure 9. Elucidating the role of autoclave treatment on (a) porosity, (b) pore size distribution, (c) in-plane fiber orientation distribution, and (d) out-of-plane fiber orientation distribution. Here, 90° angle in the out-of-plane fiber orientation distribution refers to the planar or in-plane direction and X-ray microCT implies the use of CTAn® software.

in-plane fibers compared to the control sample (see [Figure 9\(c\)](#)). On the other hand, the alignment of the out-of-plane fibers has deteriorated, which plausibly resulted in a significant reduction in the filtration efficiency after five cycles of autoclave treatment (see [Figures 3 and 9\(d\)](#)).

Polypropylene is a key constituent used in meltblown layers with a melting temperature range of 130–171°C. The semi-crystalline structure of polypropylene can attain a relaxed state, which inevitably affects the filtration performance via charge relaxation or other means [43]. Since the autoclave treatment in this study was performed at 125°C, its repeated cycling caused local structural variations due to the morphological changes occurring in polypropylene fibers. The poor filtration performance of the five-cycle autoclave-treated N95 respirator corresponds to a three-cycle autoclave-treated 3 M 1870/1870+ at 121°C for 30 min, whereby the mean retention of aerosolized particles with 0.3 µm was significantly reduced [44].

Conclusions

The meltblown layers of a commercially available N95 respirator have been analyzed for filtration performance after decontaminating it with one and five cycles of liquid hydrogen peroxide, ultraviolet radiation, moist heat, and aqueous soap solution treatments. Specifically, this work assisted in simulating the significant proportions of infectious particles generated and spread under speaking conditions, exceedingly with velocities up to 100 times greater than set under the standard test conditions. X-ray microCT analysis unraveled the local structural heterogeneities of the meltblown nonwovens that tended to grow with various treatment modalities. It was also revealed that the structural integrity obtained merely via visual observation might not truly represent the filtration performance in certain decontamination treatments. Although the structural integrity was found to be preserved in autoclave-treated meltblown nonwovens after the first treatment cycle, the filtration performance of the decontaminated N95 respirator was severely affected. On the other hand, five cycles of solution-based treatments (liquid H₂O₂ and aqueous soap) were most detrimental to the structure of the meltblown layers and significantly reduced the filtration efficiency of N95 respirators. After treating with one and five cycles of UV radiation, the filtration performance corroborated well with the structural information obtained via X-ray microCT analysis. It is worth mentioning that UV radiation may not decontaminate the inner layers of N95 respirators [45]. Accordingly, the UV treatment may be suitable for the sanitation of lightly contaminated rather than soiled N95 respirators. The outcomes of our work assist us in recommending that the local structural inhomogeneities created after repeated treatment cycles limit the use of repeated decontamination cycles of the N95 respirators. Particularly, the aqueous soap solution treatment should be avoided entirely in view of the structural delamination and entrapment of soap particles observed even in the initial cycles. In the past, some of the investigated decontamination methods have successfully deactivated the SARS-CoV-2 virus [23]. Future research efforts can be directed towards correlating our results with the virus inactivation especially using the decontamination methods at lower cycles.

Acknowledgments

Clemson University is acknowledged for generous allotment of computational time on Palmetto cluster. FW and UDS thank M Azimian, P Eichheimer, and J Becker for valuable discussions on the use of GeoDict. We also acknowledge Prof Ashwini Agrawal and Prof Manjeet Jassal for providing the necessary characterization facilities at SMITA Research Lab, IIT Delhi. RRN, PK, and SY gratefully acknowledge the support of Prof Sangeeta Talwar, Director-Principal, Maulana Azad Institute of Dental Sciences, New Delhi, India. The valuable comments of Dr PV Kameswara Rao about X-ray micro-computed tomography analysis are also acknowledged.

Declaration of conflicting interests

The author(s) declared no potential conflicts of interest with respect to the research, authorship, and/or publication of this article.

Funding

The author(s) disclosed receipt of the following financial support for the research, authorship, and/or publication of this article: The work was financially supported by Indo-Hungarian Joint Research project no. INT/HUN/P-18/2017 (2017-2.3.7-TÉT-IN- 2017-00008), the Hungarian National Research, Development and Innovation Office through the GINOP-2.3.3-15-2016-00010 project, and the US National Science Foundation under awards OIA-1655740 and DMR-1944942. Any opinions, findings and conclusions or recommendations expressed in this material are those of the author(s) and do not necessarily reflect those of the National Science Foundation.

ORCID iDs

Ulf Schiller  <https://orcid.org/0000-0001-8941-1284>

Amit Rawal  <https://orcid.org/0000-0003-4132-643X>

References

1. Volz E, Mishra S, Chand M, et al. Transmission of SARS-CoV-2 lineage B.1.1.7 in England: insights from linking epidemiological and genetic data. *Preprint at medRxiv*. 2021. DOI: [10.1101/2020.12.30.20249034](https://doi.org/10.1101/2020.12.30.20249034).
2. Tegally H, Wilkinson E, Giovanetti M, et al. Emergence and rapid spread of a new severe acute respiratory syndrome-related coronavirus 2 (SARS-CoV-2) lineage with multiple spike mutations in South Africa. *Preprint at medRxiv* 2020. DOI: [10.1101/2020.12.21.20248640](https://doi.org/10.1101/2020.12.21.20248640).
3. Classification of Omicron (B.1.1.529): SARS-CoV-2 variant of concern, [https://www.who.int/news/item/26-11-2021-classification-of-omicron-\(b.1.1.529\)-sars-cov-2-variant-of-concern](https://www.who.int/news/item/26-11-2021-classification-of-omicron-(b.1.1.529)-sars-cov-2-variant-of-concern) (2022, accessed 22 January 2022).
4. Hoffmann M, Hofmann-Winkler H, Krüger N, et al. SARS-CoV-2 variant B.1.617 is resistant to bamlanivimab and evades antibodies induced by infection and vaccination. *Cell Rep* 2021; 36: 109415.
5. World Health Organization. Coronavirus disease (COVID-19) advice for the public: When and how to use masks. <https://www.who.int/emergencies/diseases/novel-coronavirus-2019/advice-for-public/myth-busters> (2021, accessed 26 March 2021)

6. World Health Organization. Advice on the use of masks in the context of COVID-19. <https://apps.who.int/iris/handle/10665/331693> (2020, accessed 6 April 2020).
7. Atulgan Türkmen B. Life cycle environmental impacts of disposable medical masks. *Environ Sci Pollut Res* 2021; 1–11.
8. Lee HR, Liao L, Xiao W, et al. Three-dimensional analysis of particle distribution on filter layers inside N95 respirators by deep learning. *Nano Letters* 2020; 21: 651–657.
9. Dugdale CM and Walensky RP. Filtration efficiency, effectiveness, and availability of N95 face masks for COVID-19 prevention. *JAMA Intern Med* 2020; 180: 1612–1613.
10. Sickbert-Bennett EE, Samet JM, Clapp PW, et al. Filtration efficiency of hospital face mask alternatives available for use during the COVID-19 pandemic. *JAMA Intern Med* 2020; 180: 1607–1612.
11. Lee AWL, Neo ERK, Khoo Z-Y, et al. Life cycle assessment of single-use surgical and embedded filtration layer (EFL) reusable face mask. *Resour Conserv Recy* 2021; 170: 105580.
12. Bergman MS, Viscusi DJ, Heimbuch BK, et al. Evaluation of multiple (3-cycle) decontamination processing for filtering facepiece respirators. *J Eng Fibers Fab* 2010; 5: 33–41.
13. Bhattacharjee S, Bahl P, Chughtai AA, et al. Last-resort strategies during mask shortages: optimal design features of cloth masks and decontamination of disposable masks during the COVID-19 pandemic. *BMJ Open Respir Res* 2020; 7: e000698.
14. Burkhart CG. Ozone disinfectants like SoClean CPAP sanitizer can be used to sterilize cloth and N95 masks in the protection against COVID-19. *Open Dermatol J* 2020; 14: 14–15.
15. Farsi D, Mofidi M, Mahshidfar B, et al. Consider the options; can decontamination and reuse be the answer to N95 respirator shortage in COVID-19 pandemic? *Front Emerg Med* 2020; 4: e41.
16. Fisher EM, Williams JL and Shaffer RE. Evaluation of microwave steam bags for the decontamination of filtering facepiece respirators. *PloS One* 2011; 6: e18585.
17. Li DF, Cadnum JL, Redmond SN, et al. It's not the heat, it's the humidity: effectiveness of a rice cooker-steamer for decontamination of cloth and surgical face masks and N95 respirators. *Am J Infect Control* 2020; 48: 854–855.
18. Ou Q, Pei C, Chan Kim S, et al. Evaluation of decontamination methods for commercial and alternative respirator and mask materials - view from filtration aspect. *J Aerosol Sci* 2020; 150: 105609.
19. Smith JS, Hanseler H, Welle J, et al. Effect of various decontamination procedures on disposable N95 mask integrity and SARS-CoV-2 infectivity. *J Clin Trans Sci* 2020; 5: e10.
20. Viscusi DJ, Bergman MS, Eimer BC, et al. Evaluation of five decontamination methods for filtering facepiece respirators. *Ann Occup Hyg* 2009; 53: 815–827.
21. Viscusi DJ, Bergman MS, Novak DA, et al. Impact of three biological decontamination methods on filtering facepiece respirator fit, odor, comfort, and donning ease. *J Occup Environ Hyg* 2011; 8: 426–436.
22. Wang D, Sun B-C, Wang J-X, et al. Can masks be reused after hot water decontamination during the COVID-19 pandemic? *Engineering* 2020; 6: 1115–1121.
23. Kumar A, Kasloff SB, Leung A, et al. Decontamination of N95 masks for re-use employing 7 widely available sterilization methods. *PloS One* 2020; 15: e0243965.
24. Vejerano EP and Ahn J. A letter to reconsider the conditions for testing decontaminated N95 respirators for emergency reuse to address shortage. *Aerosol Air Qual Res* 2020; 20: 1713–1715.

25. O'Kelly E, Pirog S, Ward J, et al. Ability of fabric face mask materials to filter ultrafine particles at coughing velocity. *BMJ Open* 2020; 10: e039424.
26. Chao CYH, Wan MP, Morawska L, et al. Characterization of expiration air jets and droplet size distributions immediately at the mouth opening. *J Aerosol Sci* 2009; 40: 122–133.
27. Das KP, Sharma D, Saha S, et al. From outbreak of COVID-19 to launching of vaccination drive: invigorating single-use plastics, mitigation strategies, and way forward. *Environ Sci Pollut Res* 2021; 28: 55811–55845.
28. Hao W, Xu G and Wang Y. Factors influencing the filtration performance of homemade face masks. *J Occup Environ Hyg* 2021; 18: 128–138.
29. Shukla S, Kumar V, Kameswara Rao PV, et al. Probing the three-dimensional porous and tortuous nature of absorptive glass mat (AGM) separators. *J Energy Storage* 2020; 27: 101003.
30. Sharma S, Rawal A, Tóth IY, et al. Superhydrophobic self-similar nonwoven-titanate nanostructured materials. *J Colloid Interf Sci* 2021; 598: 93–103.
31. Sharma S, Wang F, Rao PVK, et al. Unfolding the effects of decontamination treatments on the structural and functional integrity of N95 respirators via numerical simulations. *Sci Rep* 2022; 12: 4191.
32. Liao L, Xiao W, Zhao M, et al. Can N95 respirators be reused after disinfection? how many times? *ACS Nano* 2020; 14: 6348–6356.
33. Viscusi DJ, King WP and Shaffer RE. Effect of decontamination on the filtration efficiency of two filtering facepiece respirator models. *J Inter Soc Respir Prot* 2007; 24: 93–107.
34. Fotovati S, Tafreshi HV and Pourdeyhimi B. Influence of fiber orientation distribution on performance of aerosol filtration media. *Chem Eng Sci* 2010; 65: 5285–5293.
35. Juang PSC and Tsai P. N95 respirator cleaning and reuse methods proposed by the inventor of the N95 mask material. *J Emerg Med* 2020; 58: 817–820.
36. Fischer RJ, Morris DH, van Doremalen N, et al. Effectiveness of N95 respirator decontamination and reuse against SARS-CoV-2 virus. *Emerg Infect Dis* 2020; 26: 2253–2255.
37. Lindsley WG, Martin SB Jr, Thewlis RE, et al. Effects of ultraviolet germicidal irradiation (UVGI) on N95 respirator filtration performance and structural integrity. *J Occup Environ Hyg* 2015; 12: 509–517.
38. Polkinghorne A and Branley J. Evidence for decontamination of single-use filtering facepiece respirators. *J Hosp Infect* 2020; 105: 663–669.
39. Jensen MM. Inactivation of airborne viruses by ultraviolet irradiation. *Appl Microbiol* 1964; 12: 418–420.
40. Jakab GJ and Knight ME. Decreased influenza virus pathogenesis by infection with germicidal UV-irradiated airborne virus. *Environ Int* 1982; 8: 415–418.
41. Heimbuch BK, Wallace WH, Kinney K, et al. A pandemic influenza preparedness study: use of energetic methods to decontaminate filtering facepiece respirators contaminated with H1N1 aerosols and droplets. *Am J Infect Control* 2011; 39: e1–e9.
42. Rutala WA and Weber DJ. Infection control: the role of disinfection and sterilization. *J Hosp Infect* 1999; 43: S43–S55.
43. Campos RK, Jin J, Rafael GH, et al. Decontamination of SARS-CoV-2 and other RNA viruses from N95 level meltblown polypropylene fabric using heat under different humidities. *ACS Nano* 2020; 14: 14017–14025.

44. Bopp NE, Bouyer DH, Gibbs CM, et al. Multicycle autoclave decontamination of N95 filtering facepiece respirators. *Appl Biosafety* 2020; 25: 150–156.
45. Kayani BJ, Weaver DT, Gopalakrishnan V, et al. UV-C tower for point-of-care decontamination of filtering facepiece respirators. *Am J Infect Control* 2021; 49: 424–429.